Ilka Hamann[1,2], Nobuhiko Azuma[1], Sepp Kipfstuhl[2]

[1]Nagaoka University of Technology, Nagaoka, Japan
[2]Alfred-Wegener-Institute of Polar and Marine Research, Bremerhaven, Germany

Microstructural deformation features in artificially deformed ice and in polar ice cores (EDML, Antarctica)

Introduction

Ice of polar ice sheets is an important information source for studying the past climate. For a correct interpretation of the age of the ice knowledge on flow and deformational processes following the deposition is essential.

Recently obtained data on sub-grain boundaries (sGB) of the deep ice core from EPICA-Dronning Maudland (Hamann et al. in prep., Figure 1 and 2) reveal that an onset of polygonization/sub-grain rotation recrystallization or an onset of migration recrystallization cannot be found. Indeed this study shows that sub-grain formation is active in any depth of EDML ice core, which indicates that the classical tripartition of recrystallization regimes (1. Grain growth, 2. Polygonization/sub-grain rotation recrystallization, 3. Migration recrystallization), which is the standard conception (e.g. Duval 2000), is not easily applicable here and has to be reconsidered.

In order to understand the sGB evolution with ongoing deformation under controlled conditions, creep experiments following standard procedures have been conducted and creep test samples have been prepared as thin sections to investigate microstructures (Kipfstuhl et al. submitted).

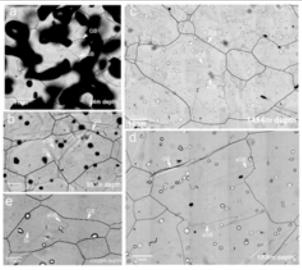

Figure 1: Examples of microstructures in EDML ice core. Grain boundaries (GB), slip lines (SL) and sub-grain boundaries (sGB) are indicated. Lower right corner shows the depth of the samples. Different grey values of features in the same picture are due to size of the etch groove produced by sublimation depending on number of bonding neighbours of atoms (viz. order of the region, number of dislocations). The different grey values have been interpreted as different stages of sGB formation (light-young, dark-old) by Wang et al. 2003. Note that sGB occur in many different depth ranges and even appear very similar in shape and distribution.

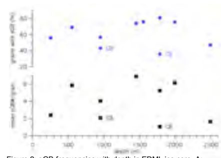

Figure 2: sGB frequencies with depth in EDML ice core. A: Frequencies of grains with sGB with respect to all grains. B: As sGB statistic on exact length of of sGB was not possible numbers of sGB per grain have been counted. Mean values are given in B. Note: frequencies of sGB-bearing grains and mean number of sGB per grain do not change with depth. Therefore an onset of polygonization by increased production of sGB could not be proofen.

Experimental results

Grain size evolution

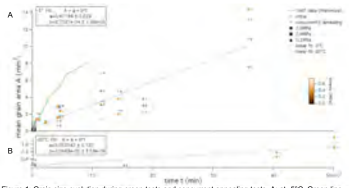

Figure 1: Grain size evolution during creep tests and concurrent annealing tests. A: at -5°C. Green line are data of grain growth experiment conducted by Nishimura. B: at -20°C. Linear fits are added after the parabolic growth law $R=k*t^{1/n}$ (A=a+b*t) (Humphreys and Hatherly 2004), to compare conditions at -5°C and -20°C.

Experimental conditions allow grain growth (Figure 1). Increase under creep is slower than under pure grain growth conditions (green data) from older experiments. Concurrently conducted annealing experiments surprisingly show approximately the same increase with time as creep tests, maybe due to sample size.

A significant difference was recognized with different temperatures.

Grain shape evolution

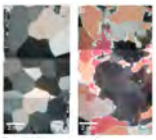

Figure 2: Photomicrographs after 8 days experiment at -4.8°C. A: Annealing only. B: Creep test with 0.6MPa stress and 10.7% total strain.

Figure 3: Schematic illustration of the definition of convex perimeter and real perimeter measured by Image Pro. This parameter is independent of size and elongation of objects and is used here to measure the regularity of grains.

Grain shapes are significantly more irregular in samples exposed to creep compared to those from annealing experiments (Figure 2). This is most obvious in higher strained samples, but measurable in all (Figure 4), b a newly invented parameter using the ratio of the real perimeter and the convex perimeter (Figure 3).

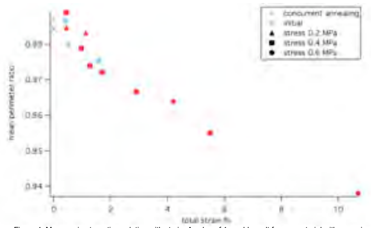

Figure 4: Mean perimeter ratio evolution with strain. A value of 1 would result from a material with no grains with inward bulges (e.g. ideal hexagons filling a surface). Red: -5°C experiments. Blue: -20°C.

Sub-grain boundary density evolution

sGB density definition: sum of all sGB lengths per area (ca. 5 mm by 6 mm of a sample surface).

It increases between 0.5 to 2% strain and reaches a steady state with approximately 3.5 mm^{-1} (Figure 5). At highest strains it increases again. With increasing strain the variability of sGB densities inside the sample increases as well. Due to slow experiment at low temperatures only few experiments could be conducted so far. However, they follow the same trend.

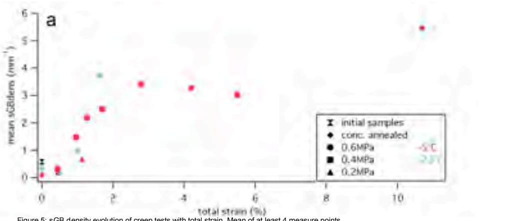

Figure 5: sGB density evolution of creep tests with total strain. Mean of at least 4 measure points.

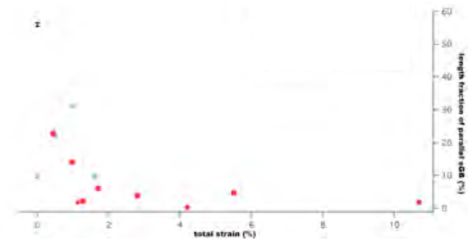

Figure 9: Frequency of parallel type of sGB in length percent with respect to all versus strain.

Sub-grain boundary types

The appearance of sGB is manifold. Variations occur in shapes and intensities (grey values). Similar to previous study on Antarctic ice sheets different types could be distinguished (Figure 6 and 7).

1 (z). Irregular (usually zigzag- or step-shaped) often appearing in networks with one reticule direction at high angle and one parallel to the basal plane trace
2 (c). Regular, straight and orthogonal or at high angle to basal plane occurring solely or in groups of few with similar orientation but at most sub-parallel
3 (p). Regular, straight and parallel to basal plane occurring in swarms of many exactly parallel sGB in one grain.

Regarding their orientation with the crystals c-axes and basal planes (Figure 7) type 2 is distinguished as tilt boundary (see Figure 8) representing the classical evolution of sGB by polygonization, type 3 as twist boundary or micro-shear zone (Bons & Jessel 1999) and type 1 seems to represent a mixture of both, e.g. alternating parts of a tilt and a twist boundary.
Not all sGB can be doubtlessly classified especially if they show no distinct shape.

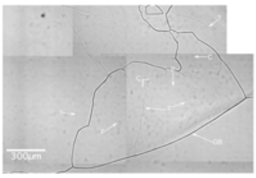

Figure 6: Example for sGB types in photomicrograph of vertical section cut from creep test sample (-4.8°C, 0.6MPa, 10.7% total strain). GB=grain boundary, p=parallel sGB, z=zigzag type sGB, C=classical polygonization type sGB, ?=bowed, not classified type sGB

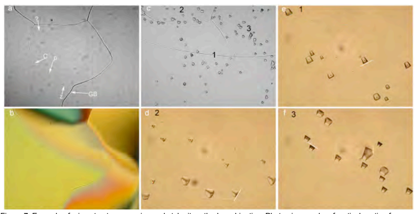

Figure 7: Example of microstructure mapping and etch pit method combination. Photomicrographs of vertical section from creep test sample (-4.8°C, 0.4MPa, 1.27% total strain.) A: Sublimated surface showing grain boundaries (GB) and different types of sGB (indication see Figure 6). B: Same sector as a, between crossed polarizers. As section is ≈3mm thick grain boundaries lie oblique in section, changing interference colours are visible along them. However clear change in orientation is visible across GB, but not across sGB. C: Same sector as a and b after application of etch pit method. Numbers indicate higher magnification detail images shown in e,d,f. White bar indicates trace of basal plane in cutting surface according to etch pit shape. (Scale: a,b,c width ~1.14mm; e,d,f width ~305µm).

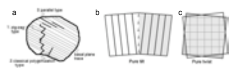

Figure 8: Schematic illustration of sGB types. A: Simplified shape. B & C: Theoretical types (after Föll, H. 2000).

Due to its eye-catching and easily recognizable nature, statistic on parallel sGB has been done. The fast decreasing evolution of their frequency can be explained in combination with the total sGB density. As sGB density is increasing with strains of 0.5 to 3 %, the fraction of parallel type is decreasing with a similar slope. This finding suggests, that mainly other types are produced in the conducted experiments. Since new other sGB are introduced the fraction of parallel ones is depleted.

Summary and Conclusions

With increasing strain from 0.5 to 2% sub-grain boundary density increases, reaching a stable value at approximately 3% strain. As strain rates reached a steady state at ca. 2 to 3% during these experiments, an explanation might be the following. The decreasing trend of the creep rate corresponds to the evolution of the substructure of the crystal, namely the production of dislocation walls and sub-grain boundaries. During primary transient creep the strain rate decreases continuously, which means that the deformation speed slows down, i.e. the material hardens. Taking into account that the deformation is to a large extent accomplished by introduction and movement of dislocations, one cause for this decrease of deformation rate is the production of obstacles, which hinder the motion of dislocations. Most common obstacles for dislocation, apart from impurities (which are absent here as pure ice is used) are dislocation walls and sub-grain boundaries. As the production of such obstacles continues the deformation rate keeps decreasing until a steady amount of obstacles is reached. This probably falls together with the achievement of maximum value of the sub-grain boundary density. As dislocations cannot move freely stress must be accumulating around obstacles. Due to the fact that deformation rate increases again at some point a new process must take over the main deformation activity. This might be rotation of crystals or grain boundary migration. That grain boundary migration intensifies and starts to dominate can be observed by the grain shape parameter.

Observations of microstructures from samples deformed by creep experiments reveal information on the formation of these features. During experiments under conditions, which allow grain growth, the grain shape changes significantly with increasing strain. The grains become more irregular with bulging grain boundaries, indicating that grain boundary migration is at least partly caused by internal strain energy differences. This is the case in experiments conducted at high temperature (-5°C) as well as under low temperatures (-20°C), where migration recrystallisation was not expected according to standard conceptions.

Acknowledgements

This study was done during a one-year research stay in Azuma-Laboratory at NagaokaUniversity of Technology in Japan. I wish to express appreciation to the laboratory members (Dr. M. Takada, A. Shigekuni, Y. Oba, T.Kokure, T. Nakamura, K. Oba, K. Anno, H. Kobayashi and many others), who helped me in so manifold ways. Technical and life support were invaluable. I thank Ch.Weikusat for patience and staying power during conducting the main part of the image analysis.

References

Bons, P.D., Jessell, M.W. 1999. Micro-shear zones in experimentally deformed OCP. J. Struct. Geol. 21, 323-334.
Duval, P. 2000. Deformation and dynamic recrystallization of ice in polar ice sheets. in: Physics of ice core records. p. 103-113. ed. T. Hondoh. Hokkaido University Press.Sapporo.
Föll, H. 2000. Defects in Crystals. Hyperscript. www.techfak.uni-kiel.de/matwis/amat/ def_en/index.html
Hamann, I., Kipfstuhl, S., Faria, S.H., Azuma, N. Sub-grain boundaries in EPICA Dronning Maudland (EDML) deep ice core. in preparation.
Humphreys, F.J. and Hatherly, M. 2004. Recrystallization and Related Annealing Phenomena. Pergamon.
Kipfstuhl, S., Hamann, I., Lambrecht, A., Freitag, J., Faria, S. H., Grigoriev, D., Azuma,N. 2006. Microstructure mapping a new method for imaging deformation-induced microstructural features of ice on the grain scale, submitted to J. Glaciol.
Wang, Y., Kipfstuhl, S., Azuma, N., Thorsteinsson, Th., Miller, H. 2003. Ice-fabrics study in the upper 1500 m of Dome C (East Antarctica) deep ice core. Ann. Glaciol. 37, 97-104.